Dalton Transactions

ROYAL SOCIETY OF CHEMISTRY

PAPER

View Article Online
View Journal | View Issue

Cite this: *Dalton Trans.*, 2021, **50**, 3529

The reactivity of an inorganic glass melt with ZIF-8†

Louis Longley, [a] Courtney Calahoo,[b] Thomas J. F. Southern, [a] Rachel C. Evans, [a] Lothar Wondraczek [b] and Thomas D. Bennett *[a]

Received 15th January 2021,
Accepted 9th February 2021

DOI: 10.1039/d1dt00152c

rsc.li/dalton

The thermal behaviour of ZIF-8, $Zn(melm)_2$ in the presence of a sodium fluoroaluminophosphate glass melt was probed through differential scanning calorimetry and thermogravimetric analysis. The structural integrity of ZIF-8 was then determined by a combination of powder X-ray diffraction, Fourier transform infra-red and ^1H nuclear magnetic resonance spectroscopy.

Introduction

Metal–organic frameworks (MOFs) are a class of materials composed of inorganic nodes joined by organic linkers.[1] The high porosity of many MOFs has led to a wide range of reported applications in gas storage, separation and catalysis,[2–4] though their microcrystalline nature has necessitated research into the formation of industrially suitable macroscale MOF architectures such as pellets, monoliths, and thin films.[5–9] Composite materials have also been produced in which the MOF crystallites are embedded in a matrix. Examples include mixed-matrix membranes (MMMs), which contain crystalline MOFs embedded within an organic polymer matrix.[10] Other composite materials reported include MOF crystal–glass composites (MOF-CGCs), formed through the combining of the crystalline and glassy states of MOFs in the same material,[11,12] or those formed by growing MOFs within activated carbon matrices.[13]

The chemical, mechanical, and thermal stabilities of functional MOF structures are also important considerations in their in-service use. Zeolitic imidazolate frameworks (ZIFs) are a subset of MOFs comprised of divalent metal cations coordinated tetrahedrally by imidazolate linkers,[14] whose stability has been extensively studied.[15] Advantages of ZIFs include their thermal stability in a wide variety of atmospheres, though care needs to be taken given their reported acid sensitivity and weak mechanical stability under ball-milling.[16,17] Further problems arise when considering stability during composite formation, such as reported correlations between incorporated ZIF amount, and mechanical failure in MMMs.[18,19]

Motivated by the promising results obtained when using a ZIF glass matrix to embed a variety of different crystalline MOFs into composite materials,[11,12,20] this work examines the possibility of expanding the MOF CGC concept, to incorporate structures in which the glass matrix is an inorganic glass. This would greatly expand the range of different matrices available, as the number of glass forming MOFs is extremely limited compared to the vast amount of known inorganic glasses. In order to form a successful MOF-inorganic CGC two criteria must be fulfilled: (i) Thermal compatibility; a processing temperature must be found at which the inorganic glass matrix is sufficiently above its glass transition (T_g), that its viscosity is low enough to promote mixing and composite formation. The temperature however, should also be low enough that the crystalline MOF remains thermally stable. (ii) Chemical compatibility; the MOF crystal inorganic glass pair must have compatible chemical bonding such that they can be bonded at the interface to produce a robust material, and no reactions which promote decomposition should occur during high temperature liquid phase mixing between the MOF and inorganic components.

Previous work has demonstrated successful composite formation between ZIF-62 ($Zn(Im)_{1.75}(bIm)_{0.25}$ Im = imidazolate $C_3H_3N_2^-$, bIm = benzimidazolate $C_7H_5N_2^-$) glass and a series of fluoroaluminophosphate glasses, where the final composite material formed was composed of separate inorganic glass and ZIF-62 glass domains which displayed bonding at the interface.[21] That work therefore indicates that these glasses are chemically compatible with ZIF-62 and therefore may imply a more general chemical compatibility with other ZIF frameworks. The lowest T_g glass of the series, **78**($[Na_2O]_{1.6}[P_2O_5]$)-**22** ($[AlO_{1.5}][AlF_3]_{0.7}$), was selected for use as a matrix material in this study because it would enable the use of the lowest processing temperatures and therefore increase the likelihood of the crystalline MOF being thermally compatible. ZIF-8, $Zn(meIm)_2$

[a]*Department of Materials Science and Metallurgy, University of Cambridge, CB3 0FS, UK. E-mail: tdb35@cam.ac.uk*
[b]*Otto Schott Institute of Materials Research, University of Jena, Fraunhoferstrasse 6, 07743 Jena, Germany*

†Electronic supplementary information (ESI) available. See DOI: 10.1039/d1dt00152c

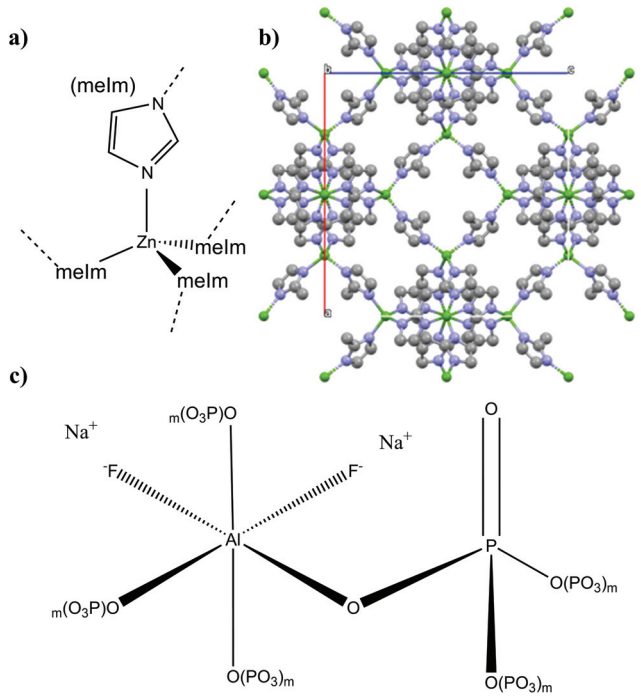

Fig. 1 (a) Local structure around the zinc centre in ZIF-8. (b) Unit cell of ZIF-8[22] viewed down the *b* axis. Element key. N: blue, C: grey, Zn: green, H omitted for clarity. (c) Schematic of the local bonding around the phosphorous and aluminium polyhedra in the inorganic glass, m indicates phosphate tetrahedra of varying polymerisation (chains, branching, *etc.*). The degree of localisation of the PO double bond depends on the local P environment.

(meIm = 2-methylimidazolate, $C_4H_5N_2^-$), was chosen as it is the 'prototypical' crystalline ZIF, whose properties and structure have been extensively studied and which is available commercially under the name Basolite® Z1200. ZIF-8 is a monolinker framework (Fig. 1a) with the cubic space group $I\bar{4}3m$ and the **sod** topology (Fig. 1b).[22,23] The local structure of the inorganic glass is composed of unconstrained tetrahedrally coordinated phosphate chains, which are strongly bonded to highly constrained, octahedrally coordinated aluminiumoxyfluoride islands, $Al(OP)_4F_2$ (Fig. 1c).[24]

Experimental

Syntheses

Synthesis of ZIF-8. ZIF-8 was synthesised using a method previously reported in the literature.[25] Zinc nitrate hexahydrate (8.75 g, 29.41 mmol) was added to 2-methylimidazole (5 g, 60.9 mmol) and both powders were dissolved in *N*,*N*-dimethylformamide (DMF) (375 ml). The mixture was covered and stirred for 1 hour at room temperature to ensure a homogenous solution. The solution was then decanted in equal volume amounts into 5 solvothermal jars, which were then heated at 120 °C for 24 hours. The product was then collected under vacuum and washed with DMF to yield a light-yellow crystalline powder (yield 64% by mol Zn).

Synthesis of the inorganic glass 78($[Na_2O]_{1.6}[P_2O_5]$)-22($[AlO_{1.5}][AlF_3]_{0.7}$). High purity reagents (optical grade) of $NaPO_3$ (66.3 g, 108.37 mmol) and AlF_3 (13.7 g, 163.2 4 mmol) were melted in a Pt crucible in an electric muffle furnace. Due to the known volatility of fluoride, care was taken to initially melt at 800 °C for one hour to allow $NaPO_3$ to melt and dissolve the AlF_3, before heating to 850 °C for 30 min to achieve homogeneity and then pouring onto a room temperature brass plate. The glass was then pulverized in a Retsch PM 100 grinder at 350 rpm with 1 min intervals for 30 min using Si_3N_4 balls (with roughly equal sample and ball volume).

Production of composite samples. The as-synthesised ZIF-8 and 78($[Na_2O]_{1.6}[P_2O_5]$)-22($[AlO_{1.5}][AlF_3]_{0.7}$) glass were added in appropriate ratios, to a total mass of 1.6 g, into a 15 ml stainless steel jar. The powders were mixed through ball milling with one 5 mm stainless steel ball for 5 minutes at 25 Hz in a Retsch MM400 grinder mill. These ball-milled powdered mixtures were then activated by soaking in *n*-butanol for 24 hours followed by vacuum filtration and heating under vacuum at 120–130 °C for 24 hours. Pellets of the evacuated powders were produced by placing 200 mg samples of the ball-milled powder mixture into a 13 mm die and compacted using 10 tons of weight applied for one minute. Heat treated samples were produced by heating approximately 10 mg samples of these pellets in a TA instruments Q600 SDT to either; (i) 450 °C for 30 minutes or (ii) 480 °C for 1 minute, under argon at 10 °C min^{-1}. Following this, samples were cooled under argon to 150 °C at 10 °C min^{-1} and then in air to room temperature at approximately 40 °C min^{-1}.

Thermal properties measurements

Thermogravimetric analysis (TGA) and differential scanning calorimetry (DSC) curves were recorded using a TA instruments Q-600 series differential scanning calorimeter. Approximately 10 mg of powdered sample was placed in open alumina crucibles. The samples were left to equilibrate for 5 minutes under argon before any heat treatment. Heating and cooling rates, under argon, of 10 °C min^{-1} were used. Data were analysed using TA Universal Analysis software, and the glass transition temperature (T_g^{Inorg}) and recrystallisation temperature (T_c^{Inorg}) were determined using the onset of the gradient change and the exothermic peak respectively.

Powder X-ray diffraction measurements (PXRD)

Data were collected using a B3 (BB) Bruker D8 DAVINCI diffractometer using Cu Kα (λ = 1.5418 Å) radiation and a LynxEye position sensitive detector in Bragg–Brentano parafocussing geometry. A 5–40° 2θ angular range was used with a step size of 0.02° and a step time of 0.75 s. Quantification of the changes in ZIF-8 crystallinity was achieved *via* peak fitting in Fityk.[26] For further details see section 1 in the ESI.†

Fourier transform infra-red spectroscopy (FTIR)

FTIR spectra of the powdered samples, approx. 2 mg, were collected on a Bruker Tensor 27 FTIR spectrometer in attenuated total reflection mode. All scans had a resolution of 4 cm^{-1}. A

background scan was collected between each sample. Quantification of relative changes in ZIF-8 and inorganic glass *via* curve fitting is discussed in section 2 of the ESI.†

^{1}H nuclear magnetic resonance (NMR) spectroscopy

Approximately 6 mg of sample powder was digested in a mixture of DCl (35%)/D_2O (0.1 ml) and DMSO-d_6 (0.6 ml) and the spectra recorded using a Bruker 500 MHz DCH Cryoprobe Spectrometer. Processing and analysis were conducted in TopSpin (3.6.1). A more detailed discussion of the D_2O peak present in all the samples can be found in section 3 in the ESI.†

Scanning electron microscopy (SEM) and image analysis

In order to get an initial estimate of the particle size of the ZIF-8, evacuated samples were prepared for SEM by mounting on pin stubs using carbon tape. The powder was then coated with palladium using an Emtech K575 sputter coater with a deposition current of 40 mA under a pressure of 1×10^{-2} mbar for approximately five minutes. These samples were then imaged using a FEI Nova NanoSEM scanning electron microscope detecting backscattered electrons. Samples of evacuated ZIF-62 $[Zn(Im)_{1.75}(bIm)_{0.25}]$ used to form composites with fluoroaluminophosphate glasses in a previous study[21] were prepared identically and also examined to provide a point of comparison. Although these images where useful for a qualitative estimate of the particle size of each framework, agglomeration made a quantitative estimate impossible. Following a method reported in the literature,[27] samples of ZIF-8 and ZIF-62 were each hand ground using a pestle and mortar for 30 seconds before being suspended in methanol *via* sonication. Two droplets of each framework suspension were pipetted on to carbon tape mounted on pin stubs. The methanol was allowed to evaporate before the samples were coated with palladium as above. These samples were imaged using a Thermo ScientificTM Phenom ProX scanning electron microscope also using backscattered electrons. Image processing to quantify particle size was conducted using Ilastik[28] and the Fiji[29] distribution of ImageJ,[30] for further details refer to the ESI.† The authors thank Lambda Photometrics Ltd for the use of this microscope.

Results and discussion

ZIF-8 and **78**$([Na_2O]_{1.6}[P_2O_5])$-**22**$([AlO_{1.5}][AlF_3]_{0.7})$, the latter of which is referred to from here on as the inorganic glass, were synthesised according to published reports (see Experimental)[21,25] and then ball milled together in the appropriate quantities to produce samples containing 5 wt%, 10 wt%, 15 wt% and 30 wt% ZIF-8 respectively. These samples were subsequently activated, and the crystallinity of the ZIF-8 confirmed through powder X-ray diffraction (PXRD) (Fig. S1 and S2 ESI†). These evacuated ball-milled mixtures are subsequently referred to as *X* wt% ZIF-8 in the text.

The thermal responses of the samples were measured during heating at 10 °C min^{-1} to 600 °C under argon (Table S1 and Fig. S3 ESI†). The differential scanning calorimetry (DSC) heating curve of the inorganic glass control was flat until a glass transition (T_g) with an onset at 350 °C, which was followed by an exotherm, with an onset of 530 °C, ascribed to recrystallisation. The heating curve of a ZIF-8 control sample was relatively featureless until around 500 °C, then became rapidly endothermic, in accordance with thermal decomposition (Fig. S3 ESI†). The 5 wt%, 10 wt% and 15 wt% ZIF-8 samples displayed similar behaviour to the inorganic glass, with T_gs between 350–360 °C followed by exotherms with onsets at approx. 520 °C (Table S1 ESI†). The recrystallisation exotherm in the 30 wt% ZIF-8 sample was much shallower and harder to unambiguously assign, this is ascribed to the increased ZIF-8 content.

The mass curves of the controls and samples were also measured by thermogravimetric analysis (TGA) (Fig. 2). The mass curve of the inorganic glass control showed a small loss of approx. 1% at 600 °C. A small peak in the mass curve was observed at approx. 540 °C, coinciding with the exotherm in the DSC curve and attributed to an increase in noise during recrystallisation. The ZIF-8 control lost approximately 3% of its mass before 500 °C, indicating successful activation of the framework. Above 500 °C, the mass loss increases sharply, in line with the rise in the DSC baseline and further confirming this as the onset of decomposition (T_d^{ZIF-8}). The 5 wt% and 10 wt% mixtures have mass curves that show intermediate behaviour between the controls, as would be expected from a rule of mixtures, however after 400 °C the 15 wt% and 30 wt% samples both lost mass at a faster rate than the ZIF-8 control.

In order to examine this unexpected effect the following construction was used; the average mass percentage signals measured from the inorganic glass control, m^{Inorg}, and ZIF-8 control, m^{ZIF} (Table S1 ESI†) were combined in the appropriate mass proportions, x^{ZIF} and x^{Inorg} respectively, as a

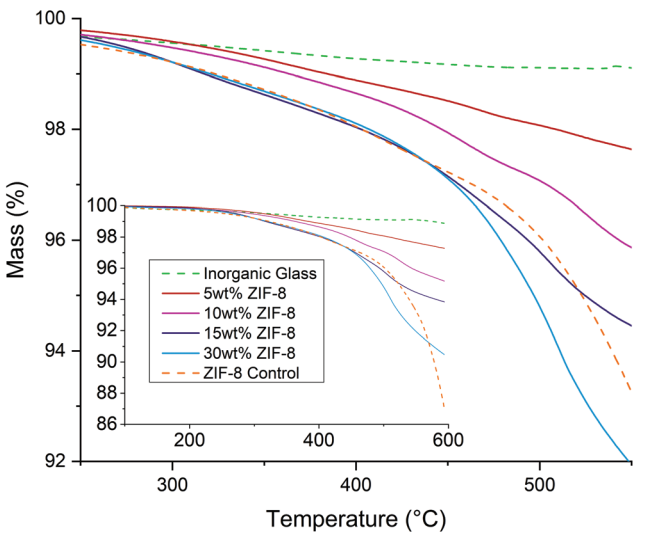

Fig. 2 Thermogravimetric analysis (TGA) curves of the ZIF-8, inorganic glass and composite samples in the region 250–550 °C. Inset: the same TGA data shown over the full measured range.

measure of the mass loss that would be expected from a non-interacting mechanical mixture of the ZIF-8 and inorganic ($m(T)^{\text{non-int}}$):

$$m(T)^{\text{non-int}} = x^{\text{ZIF}} m(T)^{\text{ZIF}} + x^{\text{Inorg}} m(T)^{\text{Inorg}} \quad (1)$$

This can then be subtracted from the mass signal directly measured for each of the mixtures in order to approximate the mass loss due to interaction between the inorganic glass and ZIF-8 ($\Delta m(T)$):

$$\Delta m(T) = m(T)^{\text{mixture}} - m(T)^{\text{non-int}} \quad (2)$$

The results of this calculation (Fig. 3) reveal that below 300 °C all $\Delta m(T)$ values are near zero, indicating relatively little interaction between the ZIF-8 and inorganic glass powder. However, at elevated temperatures, all samples lose more mass than would be expected from a non-interacting mixture ($\Delta m < 0$). Although $\Delta m(T)$ is consistently negative above 300 °C, at $T > 400$ °C the gradient increases rapidly. Above 520 °C, *i.e.* in the region in which the ZIF-8 control decomposes on its own, $\Delta m(T)$ begins to level off.

To further investigate the origin of this effect, the *X* wt% ZIF-8 samples were compressed into pellets to promote production of mechanically robust composites (see Experimental). Heat treatments of 450 °C for 30 minutes and 480 °C for 1 minute were selected as a compromise between promoting flow in the inorganic glass to join the ZIF-8 and glass together into a solid body, while avoiding decomposition of the ZIF-8 and recrystallisation of the inorganic glass. These samples were produced by heating in a DSC-TGA experiment (see Experimental).

PXRD was then conducted on the *X* wt% ZIF-8 composites, as well as the ZIF-8 and the inorganic glass controls before and after heat treatment (Fig. S4–S9 ESI†). The area under the three most intense peaks of the ZIF-8, at approximately 7.3, 12.7 and 18.0° 2θ, was used as metric for the relative change in crystallinity across the series (see section 1 in ESI†), and expressed as a fractional percentage of the peak area in the evacuated, ball-milled ZIF-8. The results show that some crystallinity is lost on pelletisation in the case of the ZIF-8 control and the 30 wt% ZIF-8 sample, but relatively little change is observed in the 5, 10 and 15 wt% ZIF-8 samples (Fig. 4, Table S2 ESI†). This difference is ascribed to the effect of the relatively dense and rigid inorganic glass, which shields the ZIF-8 from some applied stress. The 30 wt% sample displays far less stress-shielding than the other samples due to its higher fraction of ZIF-8; estimated as being over 50% by volume using densities reported in the literature.[21,31]

These results also show that while the crystallinity of the ZIF-8 control did not decrease further on heating, the crystallinity of all the *X* wt% ZIF-8 samples was reduced on heat treatment, with some samples appearing completely amorphous after heat treatment (Fig. 4, Table S2 ESI†).

ZIF-8 decomposition at elevated temperatures and in different atmospheres has previously been studied by FTIR spectroscopy.[32] FTIR of the ZIF-8 control samples contained peaks matching those recorded in the literature for as-synthesised ZIF-8, except for a broad peak at approximately 3000 cm^{-1}, due to O–H bonding, the absence of which in these samples is attributed to framework activation (Fig. S10 ESI†). The FTIR spectra of the ZIF-8 controls were unchanged upon heat treatment (Fig. S10 ESI†). The inorganic glass controls showed very broad absorbances (Fig. S11 ESI†), which is typical of IR spectroscopy on glasses where the high degree of structural disorder leads to a wide variety of similar vibrational modes.[33] The positions of these peaks were found to match those reported for other polymeric phosphates (Fig. S11 ESI†).[33,34] The heat-treated and pellet pressed inorganic glass controls also showed very little change. A band at approximately 2300 cm^{-1}, which is observed in all samples

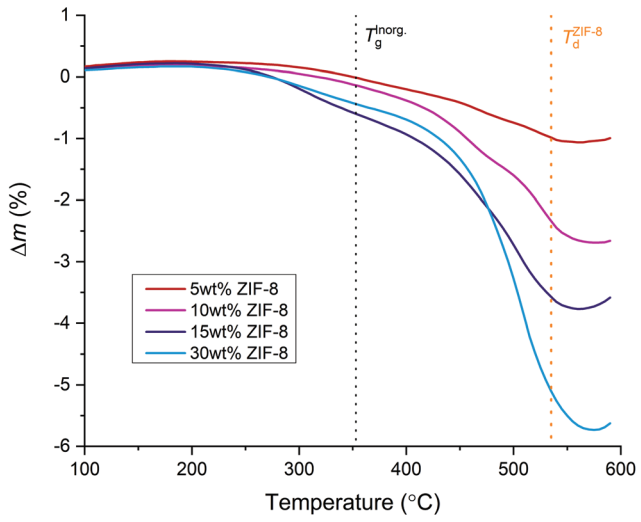

Fig. 3 $\Delta m(T)$ for the *X* wt% ZIF-8 samples. The glass transition temperature of the inorganic glass (T_g^{Inorg}) and the approximate onset of ZIF-8 decomposition as measured from the control (T_d^{ZIF-8}) are indicated.

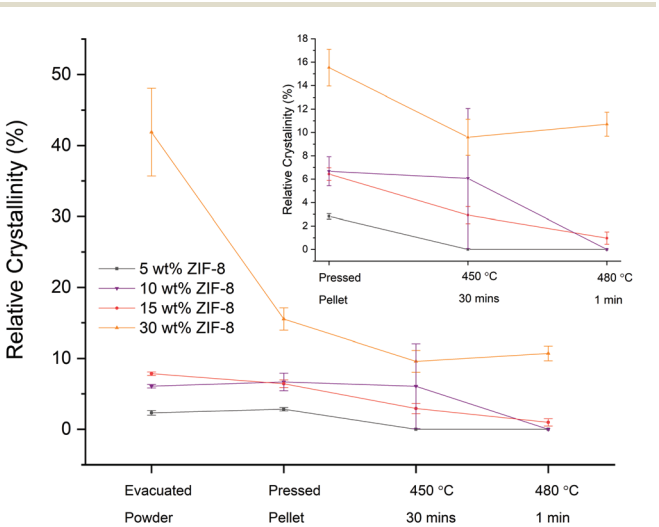

Fig. 4 Change in crystallinity, relative to the ball-milled evacuated ZIF-8 control. Inset: the heat treated and pellet pressed samples.

and controls, though with very variable intensity, was ascribed to atmospheric CO_2 present in the open measurement set-up.[35]

In order to investigate the changes in the relative proportions of the inorganic glass and ZIF-8 in the samples during heat treatment, the area under the ZIF-8 peak at 1440 cm^{-1} and the inorganic glass peak at 910 cm^{-1} were integrated and a ratio taken (see section 2 in ESI†). These ratios show a general decrease in ZIF-8 content on heat treatment (Fig. S12–23, Table S3 ESI†). Peaks at 904 cm^{-1}, 1041 cm^{-1}, 1251 cm^{-1} and 2200 cm^{-1} are reported in the literature to appear upon decomposition, and are ascribed to disordering in the CN bonding and the formation of aliphatic amines.[32] Some of these peaks are indeed observed in the 10 wt%, 15 wt% and 30 wt% samples on heat treatment, though due to the inorganic glass background their unambiguous assignment is difficult. They are not observed in the 5 wt% sample, which is due to the overall low ZIF-8 content (Fig. S12–23 ESI†).

To confirm that the reduction in Bragg scattering in PXRD, and relative ZIF-8 peak intensity in FTIR coincides with a reduction in the amount of 2-methylimidazole, ^{1}H NMR spectroscopy was conducted on the 15 wt% ZIF-8 sample heated to 450 °C for 30 minutes (Fig. S24–28, Tables S4 and S5 ESI†). This sample was selected because it showed a substantial drop in ZIF-8 content, as measured by PXRD and FTIR. Although peaks matching those of the ZIF-8 control were observed, their integration trace had fallen by a factor of five relative to the non-heat-treated sample, using the DMSO-d6 peak as a standard (Fig. S24–28, Tables S4 and S5 ESI†). This confirms the results of the FTIR experiments, showing that the 2-methylimidazolate linker is destroyed during heat treatment, and indicates that the reduction in the intensity of the Bragg peaks is due to decomposition of the linker and not to thermal amorphisation of the framework. However, no decomposition products could be observed in the ^{1}HNMR results. This is explained by decomposition being reported as proceeding *via* formation of tertiary amines with no H environments.[32]

The results presented here indicate that an interaction occurs between ZIF-8 and the inorganic glass, which has a destabilising effect on the ZIF framework. The fact that $\Delta m(T)$ becomes rapidly more negative at temperatures above 400 °C, *i.e.* approx. 50 °C above T_g^{inorg}, is consistent with increasing decomposition due to a more intimate mixing between the inorganic and the ZIF, *i.e.* mixing occurring when the inorganic glass is sufficiently fluid. PXRD data indicate the reduction or complete loss of crystallinity on heating the pellet pressed *X* wt% samples. FTIR and ^{1}H NMR confirm that this loss is due to linker decomposition rather than amorphisation of ZIF-8. New peaks that emerged during heat-treatment in the FTIR spectra are consistent with those previously reported as being observed during decomposition of ZIF-8 in the literature.[32] This indicates that decomposition in the inorganic ZIF-8 mixtures may proceed *via* a similar mechanism to decomposition of the pure ZIF-8, but that it occurs at a lower temperature due to the presence of the inorganic glass.

Previous work has shown that ZIF-62 formed stable composites with this inorganic glass and so the instability of ZIF-8, a framework with a similar chemistry, is somewhat surprising.[21] SEM on evacuated and dispersed samples of both frameworks coupled with image processing and analysis (see section 4 ESI†) confirmed that this difference was not due to a drastically smaller particle size in the ZIF-8 relative to the ZIF-62, with the ZIF-8 in this study having a comparable range of particle sizes to the ZIF-62 used previously (Fig. S29–S34 ESI†).

This leaves differences which are intrinsic to the two frameworks, namely linker chemistry and framework topology, which have both been found to be key factors in determining framework stability.[36] More dense frameworks, for example, are reported as being more stable due to enhanced dispersion interactions between the linkers,[37] and so the instability of ZIF-8 relative to ZIF-62 could therefore be ascribed to its lower framework density.[22,38] The addition of a methyl group to the imidazole ring has also been shown by molecular dynamics simulations to have a substantial effect on the high-temperature dynamics around the Zn centre[39] and so will also have an effect on the linker reactivity.

These findings illustrate the difficulty of finding chemically compatible MOF-inorganic glass pairs. Interfacial interactions are inherently difficult to characterise due to the small size of interfacial regions relative to the bulk of both components in the composite. This means that interface specific interactions, though vital to successful composite formation, are often not observed by bulk experimental methods. Moreover, interactions at the interfaces involving decomposition may be even more difficult to fully characterise due to the transient nature of the decomposing ZIF framework which makes *ex situ* measurement difficult. The results here underscore the inherent difficulty of predicting chemical compatibility ahead of time.

Conclusions

In conclusion the presence of an inorganic glass, **78** ($[Na_2O]_{1.6}[P_2O_5]$)-**22**($[AlO_{1.5}][AlF_3]_{0.7}$), was found to have a deleterious effect on the thermal stability of the ZIF-8 framework. However the combination of a crystalline MOF component with an apposite inorganic glass to create a porous composite with the high specific surface areas and chemical selectivity typical of MOFs, combined with the rigidity, processability and mechanical properties of inorganic glasses remains a worthwhile research objective. The use of low T_g inorganics would allow processing at lower temperatures in which the MOF component is more intrinsically stable. However the nature of the viscosity change of the inorganic glass above T_g, *i.e.* strong *vs.* fragile glass formers,[40] may play a more important role than absolute processing temperature, as may the availability of oxygen anions in the melt, as measured by the optical basicity of the glass.[41] Both MOFs and glasses display a wide variety of chemistries and physical properties, indicating that the scope

of potential composite pairs is likely to be very broad.[40,42] This study, combined with the fact that previous work had illustrated the compatibility of the same inorganic glass with another ZIF framework, also illustrates the difficulty of predicting the compatibility of a given MOF-inorganic glass pair *a priori*, and therefore underscores the need for a set of general research guidelines are to help guide further research efforts. Once compatible MOF crystal – inorganic glass pairings have been discovered, it is hoped that studies can also expand to examine the functional properties of such composite materials, *i.e. via* gas sorption studies, however in this case the inherent instability of the samples precluded such work. However, in spite of this, the authors hope that these results demonstrate an experimental methodology for determining the viability of a given MOF-inorganic glass pair, and that such a methodology can be used as the basis of a screening process to find compatible chemistries in the future.

Author contributions

LL, CC and TDB designed the project. LL wrote the manuscript with input from TDB, RCE, LW, CC and TJFS. Synthesis of the inorganic glass was conducted by CC. LL synthesised the ZIF-8 and produced the composite samples. Thermal analysis, PXRD and FTIR was conducted by LL. Sample preparation for NMR was conducted by LL, with the measurements being done by departmental technician and the results interpreted by LL and CC. SEM preparation and data analysis were conducted by TJFS with assistance from LL.

Conflicts of interest

There are no conflicts to declare.

Acknowledgements

This project received funding from the European Research Council (ERC) under the European Union's Horizon 2020 research and innovation program (ERC grant UTOPES, grant agreement no. 681652). T.D.B acknowledges the Royal Society for a University Research Fellowship (UF150021), and a research grant (RSG\R1\180395). He also wishes to thank the University of Canterbury Te Whare Wānanga o Waitaha, New Zealand, for a University of Cambridge Visiting Canterbury Fellowship, and the Leverhulme Trust for a Philip Leverhulme Prize (2019). LL acknowledges the EPSRC for PhD studentship funding. TJFS thanks the EPSRC (EP/1937468) for PhD studentship funding.

Notes and references

1 G. Maurin, C. Serre, A. Cooper and G. Férey, *Chem. Soc. Rev.*, 2017, **46**, 3104–3107.
2 H. Sato, W. Kosaka, R. Matsuda, A. Hori, Y. Hijikata, R. V. Belosludov, S. Sakaki, M. Takata and S. Kitagawa, *Science*, 2014, **343**, 167–170.
3 H. Zhong, M. Ghorbani-Asl, K. H. Ly, J. Zhang, J. Ge, M. Wang, Z. Liao, D. Makarov, E. Zschech, E. Brunner, I. M. Weidinger, J. Zhang, A. V. Krasheninnikov, S. Kaskel, R. Dong and X. Feng, *Nat. Commun.*, 2020, **11**, 1409.
4 Z. Chen, P. Li, R. Anderson, X. Wang, X. Zhang, L. Robison, L. R. Redfern, S. Moribe, T. Islamoglu, D. A. Gómez-Gualdrón, T. Yildirim, J. F. Stoddart and O. K. Farha, *Science*, 2020, **368**, 297–303.
5 M. S. Denny, J. C. Moreton, L. Benz and S. M. Cohen, *Nat. Rev. Mater.*, 2016, **1**, 16078.
6 B. Bueken, N. Van Velthoven, T. Willhammar, T. Stassin, I. Stassen, D. A. Keen, G. V. Baron, J. F. M. Denayer, R. Ameloot, S. Bals, D. De Vos and T. D. Bennett, *Chem. Sci.*, 2017, **8**, 3939–3948.
7 S. Furukawa, J. Reboul, S. Diring, K. Sumida and S. Kitagawa, *Chem. Soc. Rev.*, 2014, **43**, 5700–5734.
8 O. Shekhah, J. Liu, R. A. Fischer and C. Wöll, *Chem. Soc. Rev.*, 2011, **40**, 1081–1106.
9 S. Li, R. Limbach, L. Longley, A. Shirzadi, J. C. Walmsley, D. N. Johnstone, P. A. Midgley, L. Wondraczek, R. Limbach, A. A. Shirzadi and T. D. Bennett, *J. Am. Chem. Soc.*, 2019, **141**, 1027–1034.
10 A. Kertik, L. H. Wee, M. Pfannmoeller, S. Bals, J. Martens and I. F. J. Vankelecom, *Energy Environ. Sci.*, 2017, **10**, 2342–2351.
11 J. Hou, C. W. Ashling, S. M. Collins, A. Krajnc, C. Zhou, L. Longley, D. N. Johnstone, P. A. Chater, S. Li, M.-V. Coulet, P. L. Llewellyn, F.-X. Coudert, D. A. Keen, P. A. Midgley, G. Mali, V. Chen and T. D. Bennett, *Nat. Commun.*, 2019, **10**, 2580.
12 C. W. Ashling, D. N. Johnstone, R. N. Widmer, J. Hou, S. M. Collins, A. F. Sapnik, A. M. Bumstead, P. A. Midgley, P. A. Chater, D. A. Keen and T. D. Bennett, *J. Am. Chem. Soc.*, 2019, **141**, 15641–15648.
13 L. N. McHugh, A. Terracina, P. S. Wheatley, G. Buscarino, M. W. Smith and R. E. Morris, *Angew. Chem., Int. Ed.*, 2019, **8**, 11747–11751.
14 H. Hayashi, A. P. Côté, H. Furukawa, M. O'Keeffe and O. M. Yaghi, *Nat. Mater.*, 2007, **6**, 501–506.
15 K. S. Park, Z. Ni, A. P. Côté, J. Y. Choi, R. Huang, F. J. Uribe-Romo, H. K. Chae, M. O'Keeffe and O. M. Yaghi, *Proc. Natl. Acad. Sci. U. S. A.*, 2006, **103**, 10186–10191.
16 S. Cao, T. D. Bennett, D. A. Keen, A. L. Goodwin and A. K. Cheetham, *Chem. Commun.*, 2012, **48**, 7805.
17 S. Bhattacharyya, R. Han, W. G. Kim, Y. Chiang, K. C. Jayachandrababu, J. T. Hungerford, M. R. Dutzer, C. Ma, K. S. Walton, D. S. Sholl and S. Nair, *Chem. Mater.*, 2018, **30**, 4089–4101.
18 E. M. Mahdi and J. C. Tan, *J. Membr. Sci.*, 2016, **498**, 276–290.
19 M. J. C. Ordoñez, K. J. Balkus, J. P. Ferraris and I. H. Musselman, *J. Membr. Sci.*, 2010, **361**, 28–37.

20 S. Li, S. Yu, S. M. Collins, D. N. Johnstone, C. W. Ashling, A. F. Sapnik, P. A. Chater, D. S. Keeble, L. N. McHugh, P. A. Midgley, D. A. Keen and T. D. Bennett, *Chem. Sci.*, 2020, **11**, 9910–9918.
21 L. Longley, C. Calahoo, R. Limbach, Y. Xia, J. M. Tuffnell, A. F. Sapnik, M. F. Thorne, D. S. Keeble, D. A. Keen, L. Wondraczek and T. D. Bennett, *Nat. Commun.*, 2020, **11**, 5800.
22 J. Cousin Saint Remi, T. Rémy, V. Van Hunskerken, S. van de Perre, T. Duerinck, M. Maes, D. De Vos, E. Gobechiya, C. E. A. Kirschhock, G. V. Baron and J. F. M. Denayer, *ChemSusChem*, 2011, **4**, 1074–1077.
23 A. Phan, C. J. Doonan, F. J. Uribe-Romo, C. B. Knobler, M. O'Keeffe and O. M. Yaghi, *Acc. Chem. Res.*, 2010, **43**, 58–67.
24 C. Calahoo, J. Petrovic, Q. H. Le, U. Werner-Zwanziger, J. Zwanziger and L. Wondraczek, *Front. Mater.*, 2019, **6**, 1–15.
25 O. Karagiaridi, M. B. Lalonde, W. Bury, A. A. Sarjeant, O. K. Farha and J. T. Hupp, *J. Am. Chem. Soc.*, 2012, **134**, 18790–18796.
26 M. Wojdyr, *J. Appl. Crystallogr.*, 2010, **43**, 1126–1128.
27 H. H. M. Yeung, A. F. Sapnik, F. Massingberd-Mundy, M. W. Gaultois, Y. Wu, D. A. X. Fraser, S. Henke, R. Pallach, N. Heidenreich, O. V. Magdysyuk, N. T. Vo and A. L. Goodwin, *Angew. Chem., Int. Ed.*, 2019, **58**, 566–571.
28 S. Berg, D. Kutra, T. Kroeger, C. N. Straehle, B. X. Kausler, C. Haubold, M. Schiegg, J. Ales, T. Beier, M. Rudy, K. Eren, J. I. Cervantes, B. Xu, F. Beuttenmueller, A. Wolny, C. Zhang, U. Koethe, F. A. Hamprecht and A. Kreshuk, *Nat. Methods*, 2019, **16**, 1226–1232.
29 J. Schindelin, I. Arganda-Carreras, E. Frise, V. Kaynig, M. Longair, T. Pietzsch, S. Preibisch, C. Rueden, S. Saalfeld, B. Schmid, J. Y. Tinevez, D. J. White, V. Hartenstein, K. Eliceiri, P. Tomancak and A. Cardona, *Nat. Methods*, 2012, **9**, 676–682.
30 M. D. Abràmoff, P. J. Magalhães and S. J. Ram, *Biophotonics Int.*, 2004, **11**, 36–41.
31 J. Tan, T. D. Bennett and A. K. Cheetham, *Proc. Natl. Acad. Sci. U. S. A.*, 2010, **107**, 9938–9943.
32 J. B. James and Y. S. Lin, *J. Phys. Chem. C*, 2016, **120**, 14015–14026.
33 Y. M. Moustafa and K. El-Egili, *J. Non-Cryst. Solids*, 1998, **240**, 144–153.
34 E. E. Metwalli, R. K. Brow and F. S. Stover, *J. Am. Ceram. Soc.*, 2001, **84**, 1025–1032.
35 K. Isokoski, C. A. Poteet and H. Linnartz, *Astron. Astrophys.*, 2013, **555**, 4–9.
36 A. M. Bumstead, M. L. Ríos Gómez, M. F. Thorne, A. F. Sapnik, L. Longley, J. M. Tuffnell, D. S. Keeble, D. A. Keen and T. D. Bennett, *CrystEngComm*, 2020, **22**, 3627–3637.
37 R. Gaillac, P. Pullumbi and F. X. Coudert, *J. Phys. Chem. C*, 2018, **122**, 6730–6736.
38 R. Banerjee, A. Phan, B. Wang, C. Knobler, H. Furukawa, M. O'Keeffe and O. M. Yaghi, *Science*, 2008, **319**, 939–943.
39 R. Gaillac, P. Pullumbi, K. A. Beyer, K. W. Chapman, D. A. Keen, T. D. Bennett and F.-X. Coudert, *Nat. Mater.*, 2017, **16**, 1149–1155.
40 A. K. Varshneya, *Fundamentals of Inorganic Glasses*, Academic Press, Inc., San Diego, 1st edn, 1994.
41 J. A. Duffy, *J. Chem. Educ.*, 1996, **73**, 1138–1142.
42 P. Z. Moghadam, A. Li, S. B. Wiggin, A. Tao, A. G. P. Maloney, P. A. Wood, S. C. Ward and D. Fairen-Jimenez, *Chem. Mater.*, 2017, **29**, 2618–2625.